Journal of Science and Technology of METALS

Tổng hợp vật liệu nano TiO_2 anatase từ kim loại Ti nhằm tăng cường hiệu quả quang xúc tác khả kiến

Facile synthesis of anatase TiO_2 nanoparticles using titanium metal and its enhanced photocatalytic activity under visible light

HÀ KIỀU TRANG[1], LÊ THỊ THƯƠNG[1], NGUYỄN THỊ TRANG[1], NGUYỄN KIM NGÀ[1], NGÔ ĐỨC QUÂN[2,*], LƯƠNG XUÂN ĐIỀN[1,*]

[1.] Viện Kỹ thuật Hóa học, Trường Đại học Bách khoa Hà Nội, Số 1 Đại Cồ Việt, Hà Nội

[2.] Viện Vật lý kỹ thuật, Trường Đại học Bách khoa Hà Nội, Số 1 Đại Cồ Việt, Hà Nội

*Email: dien.luongxuan@hust.edu.vn, quan.ngoduc@hust.edu.vn

Ngày nhận bài:2/1/2023, Ngày duyệt đăng:24/3/2023

TÓM TẮT

Bài báo này giới thiệu phương pháp sol-gel xanh để tổng hợp vật liệu nano TiO_2 (NP) trên cơ sở kim loại Ti. Sau khi được tổng hợp, NP TiO_2 được khảo sát cấu trúc, hình thái và đặc trưng quang xúc tác thông qua các kỹ thuật như nhiễu xạ Ronghen (XRD), phổ hồng ngoại (IR), hiển vị điện tử truyền qua (TEM) và phổ phản xạ khuếch tán UV-Vis (UV-Vis DRS). Việc điều chỉnh nồng độ axit oxalic giúp cải thiện đặc trưng quang xúc tác khả kiến của TiO_2 anatase. Chất xúc tác TiO_2 thu được có diện tích bề mặt lớn, khả năng hấp phụ và quang phân MB trong dải bức xạ khả kiến tốt. Đặc trưng quang xúc tác khả kiến tốt của TiO_2 được cho là do diện tích bề mặt lớn và tác động của lỗ trống ôxy.

Từ khóa: *Titan kim loại, phức Titan, TiO_2 biến tính, quang xúc tác, lỗ trống ôxy, ánh sáng khả kiến.*

ABSTRACT

A green sol-gel method was employed to synthesize TiO_2 nanoparticles (NPs) using titanium metal. The synthesized TiO_2 NPs underwent comprehensive characterization using techniques including X-ray diffraction (XRD), infrared spectroscopy (IR), transmission electron microscopy (TEM), and UV–Vis diffuse reflectance spectroscopy (UV-Vis DRS) to evaluate their structure, morphology, and spectral properties. By adjusting the amount of oxalic acid, tailored physico-chemical properties of anatase TiO_2 catalysts were achieved. The obtained TiO_2 catalysts demonstrated a high surface area, excellent absorption, and remarkable photocatalytic degradation of methylene blue under visible light irradiation. This enhancement is primarily contributed by the large surface area and oxygen vacancies.

Keywords: *Titanium metal, titanium complex, modified TiO_2, photocatalyst, oxygen vacancy, visible light.*

1. INTRODUCTION

The removal of organic pollutants from wastewater is a critical necessity due to the significant health risks they pose to the environment and living organisms [1-5]. Various methods have been developed to address this issue, including adsorption onto the surface of active materials such as activated carbon, zeolite, or metal-organic frameworks. However, these methods have their limitations and are considered discontinuous since the adsorbent or membrane needs frequent regeneration or reactivation, especially when dealing with high pollutant concentrations. An alternative approach that shows promise is the utilization of advanced oxidation processes employing heterogeneous photocatalysts [6]. This method effectively and economically degrades a wide range of water-dispersed contaminants into biodegradable and less toxic compounds. Furthermore, photocatalytic degradation processes are renowned for being environmentally friendly.

One of the most commonly used photocatalysts is titanium dioxide (TiO_2), which offers several

advantages such as high stability, non-toxicity, low cost, and a simple synthesis procedure [7-9]. However, its relatively large bandgap restricts its activity to ultraviolet (UV) light. To enable the utilization of visible light, modifications have been made to TiO_2 by incorporating metals or non-metals, such as carbon and oxygen vacancies, through suitable synthetic methods and reagents. These modified photocatalysts, known as titanium dioxide-heterojunctions, have attracted significant interest in various fields including photocatalysis, solar cells, electronic materials, cancer therapy, water and air purification. They are renowned for their high redox potential, chemical stability, and cost-effectiveness.

Ti-alkoxides, $TiCl_4$ and $Ti(SO_4)_2$ are common sources of titanium (Ti) for solution [10]. However, they pose challenges due to their strong toxicological and corrosive properties, making them difficult to handle. Another issue is the rapid hydrolysis of Ti ions, resulting in Ti compounds with poor solubility in water. Recently, T.Q. Duc et al. have successfully synthesized water-soluble Ti-complexes [11]. These complexes are environmentally friendly as they are formed using harmless organic acids known as hydroxycarboxylic acids. Consequently, significant efforts have been devoted to controlling the morphology and crystalline phase of TiO_2 powders using water-soluble Ti-complexes under hydrothermal conditions [9-11]. However, there are fewer studies that have reported on the preparation and characterization of nanopowders using water-soluble Ti-complexes through the sol-gel method. It is widely recognized that the choice of precursor plays a significant role in determining the crystalline phase and morphology of the synthesized particles. When using titanium complex precursors, factors such as the ligand or complex structure, as well as experimental conditions, have a crucial impact on the resulting crystalline phase and morphology of the synthesized nanostructures.

In this study, we employed a sol-gel treatment of a titanium oxalate complex to prepare TiO_2 catalysts with various morphologies. The influence of the oxalic acid content on the formation of crystallites, particle size, shape, and subsequent photocatalytic activity of the synthesized TiO_2 nanoparticles were thoroughly investigated.

2. EXPERIMENTAL

2.1. Materials

The experiments utilized chemical reagents sourced from commercial suppliers, ensuring their analytical purity. Additionally, distilled water was consistently employed throughout the experiments.

2.2. Synthesis of TiO_2 NPs using Ti metal

To prepare TiO_2 NPs, a sol-gel method was employed using a titanium complex with oxalic acid as a chelating agent [10,11]. In a typical synthesis, metallic titanium powder (45 mmol, 99 % purity, sourced from China) was dissolved in a cold mixture of aqueous ammonia solution (45 ml, 28 % concentration, Xilong, China) and hydrogen peroxide solution (180 ml, 30 % concentration, Xilong, China). After stirring for 3 hours and filtering out the excess reagents, a yellowish peroxo-titanic acid solution was obtained. Next, oxalic acid (sourced from Xilong, China) was added to the peroxo-titanic acid solution, resulting in a solution where the color changed from yellow to red, indicating the formation of a titanium oxalate complex. The solutions were stirred and heated at 343 K until a slightly yellow gel formed. The obtained gel was then dried at 353 K overnight. The resulting powder was ground and subjected to calcination at 573 K for 4 hours to produce TiO_2 catalysts. The sample was labeled as TiO_2_1_X (where X represents the molar ratio of oxalic acid to Ti).

2.3. Synthesis of TiO_2 NPs from $TiCl_4$

TiO_2 NPs were synthesized using a sol-gel method, employing a titanium complex with oxalic acid as the chelating agent [12]. To obtain single crystals of ammonium titanyl oxalate, a direct approach was taken. Initially, a clear, hydrolyzed solution of $TiCl_4$ in water (approximately 0.5 M) was prepared. Two equivalents of solid oxalic acid were then dissolved in this solution, followed by the careful addition of 4-5 equivalents of ammonia. The resulting solution, which remained clear, was adjusted to a pH of around 1-2. Subsequently, half the volume of ethanol was slowly added over several hours, without stirring, resulting in the formation of two slightly mixed layers. After allowing the solution to stand overnight, colorless crystals of $(NH_4)_2TiO(C_2O_4)_2.H_2O$ were obtained with a high yield (~80%). The crystals were then dried at 353 K overnight. The resulting powder was ground and calcined at 573 K for 4 hours to produce TiO_2 catalysts. This particular sample was designated as TiO_2_$TiCl_4$.

2.4. Characterization of TiO_2 NPs

The identification of the crystalline phase involved utilizing powder X-ray diffraction (XRD) analysis. The XRD measurements were conducted using an AERIS RESEARCH instrument by MALVERN PANALYTICAL, employing Cu-Kα radiation with a wavelength (λ) of 1.5406 Å. The data acquisition was performed at a scan speed of 4° per minute, with a step-size of 0.02°.

The examination of the morphology involved employing transmission electron microscopy (TEM) on a Jeol JEM-1010 instrument. To determine the Brunauer-Emmett-Teller (BET) specific surface area, nitrogen adsorption and desorption isotherms were measured at 77 K using a Micromeritics ASAP 2020 instrument. Prior to the measurement, the powders were subjected to a 4-hour degassing process under a nitrogen atmosphere at 200 °C. The identification of functional groups was accomplished using a JASCO Infrared spectrometer. Additionally, all samples underwent measurements utilizing diffuse reflectance spectroscopy on a JASCO V-750 instrument.

2.5. Photocatalytic degradation of methylene blue

The experiment begins by preparing a solution of methylene blue (MB) in a 100 ml beaker. To achieve this, 60 ml of a 15 ppm MB solution is carefully poured into the beaker. Next, 0.06 g of catalyst is added to the solution. Before the reaction commences, the solution is subjected to magnetic stirring in a dark environment for 30 minutes. This step ensures that the nanoparticles disperse evenly throughout the solution and establishes an absorption/desorption equilibrium.

Once the solution is prepared, it is time for irradiation. A visible light source, a 200 W tungsten lamp, is used for this purpose. The solution is vigorously stirred while being exposed to the light. Each reaction lasts for 1.5 hours, during which 6 ml samples of the reaction mixture are extracted at 15-minute intervals. These samples are then analyzed to determine the composition of the dye.

For analysis, an Agilent UV-Vis spectrometer (8453) is employed. Before measuring, the liquid mixture is filtered. Absorption measurements are taken at a wavelength of 664 nm, as initial scans have indicated that this wavelength corresponds to the maximum absorbance for the relevant dye concentrations. By comparing these measurements to a calibration curve, the concentrations of the dye can be determined accurately.

To assess the photocatalytic performance of the synthesized TiO_2 catalysts, a comparison was made with a commercial P25 TiO_2 catalyst (Degussa,

Evonik, 54 m^2/g) having an anatase/rutile ratio of 4/1. The sample derived from the commercial catalyst was labeled as TiO_2_P25.

3. RESULTS and DISCUSSION

3.1. Characterization of TiO_2 catalysts

3.1.1. Structure and morphology

Figure 1 displays the wide-angle XRD patterns of the as-prepared TiO_2-based catalysts. These catalysts revealed distinct diffraction peaks at angles of 25.37°, 37.05°, 37.91°, 38.67°, 48.16°, 54.05°, 55.20°, 62.8°, 68.9°, 70.4°, and 75.3°, which correspond to the diffraction of (101), (103), (004), (112), (200), (105), (211), (204), (116), (220), and (215) facets of anatase TiO_2 (JCPDS PDF#21-1272), respectively. No other crystalline titanium oxide polymorphs were observed. The diffraction peaks depicted in Figure 1 are relatively broad due to the nanoscale size of the crystals. The average crystallite sizes of the TiO_2 nanoparticles were determined using the Scherrer equation (1):

$$D = \frac{K\lambda}{\beta \mathrm{Cos}\theta}, \quad (1)$$

where D is the crystallite size, K represents the shape factor, λ is the wavelength (λ = 0.154 nm), β denotes the full width at half maximum, and θ refers to the reflection angle (here, 2θ angle of 25.37°, corresponding to the most intense diffraction peak (101)). The results are presented in Table 1. The calculated sizes were found to be 10.2 nm for TiO_2_$TiCl_4$, 5.1 nm for TiO_2_1_5, 10.9 nm for TiO_2_1_4, 13.1 nm for TiO_2_1_3, and 14.3 nm for TiO_2_1_2. Consequently, the addition of more oxalic acid leads to a reduction in the size of the TiO_2 nanomaterials prepared. These results are in line with the observation from transmission electron micrographs, illustrating the morphology of TiO_2 nanoparticles, presented in Figure 3. The images reveal a spherical-like shape with average diameters ranging from 4 to 15 nm. The nanoparticles exhibit a relatively narrow size distribution, which is a characteristic feature of the sol-gel method.

The specific surface area of the TiO_2 catalysts was determined through N_2 adsorption-desorption measurements, and the resulting isotherms are presented in Figure 2. The significant decrease in the desorption curve and the presence of a hysteresis loop at high relative pressure clearly indicated that all the as-prepared TiO_2 catalysts possessed a mesoporous structure, exhibiting representative type-IV curves [14]. The specific surface areas of TiO_2_1_2, TiO_2_1_3, TiO_2_1_4, TiO_2_1_5, and TiO_2_$TiCl_4$ were calculated to be 83, 115, 109, 192, and 161 m^2/g, respectively. These TiO_2 catalysts exhibited considerably higher surface areas, providing more reactive sites compared to commercial pure TiO_2 (Degussa P25, 54 m^2/g), indicating their superior capability to adsorb organic compounds onto their surfaces.

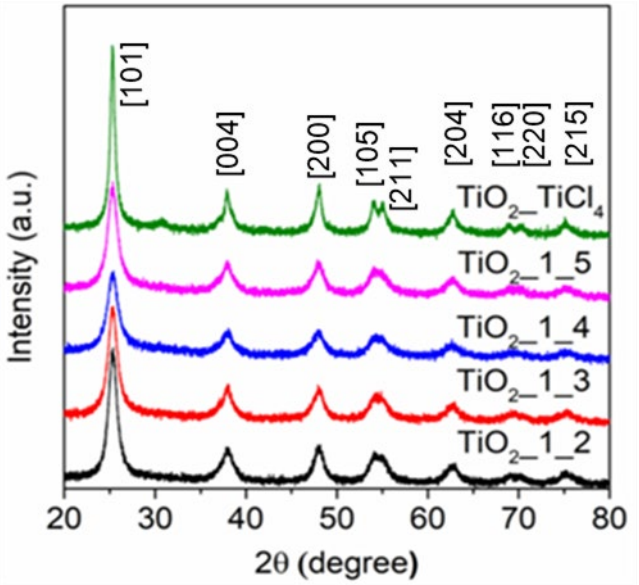

***Figure* 1.** XRD patterns of the synthesized TiO_2 catalysts: TiO_2_1_2; TiO_2_1_3; TiO_2_1_4; TiO_2_1_5; TiO_2_$TiCl_4$.

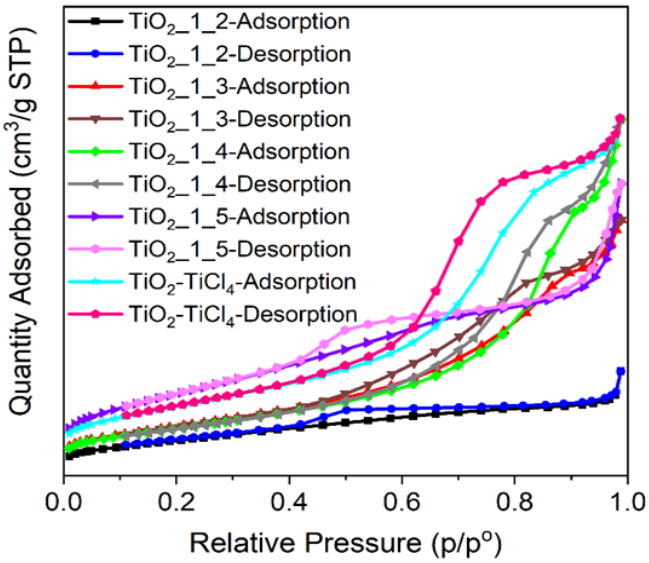

Figure 2. BET specific surface area of the synthesized TiO_2 catalysts: TiO_2_1_2; TiO_2_1_3; TiO_2_1_4; TiO_2_1_5; TiO_2_$TiCl_4$.

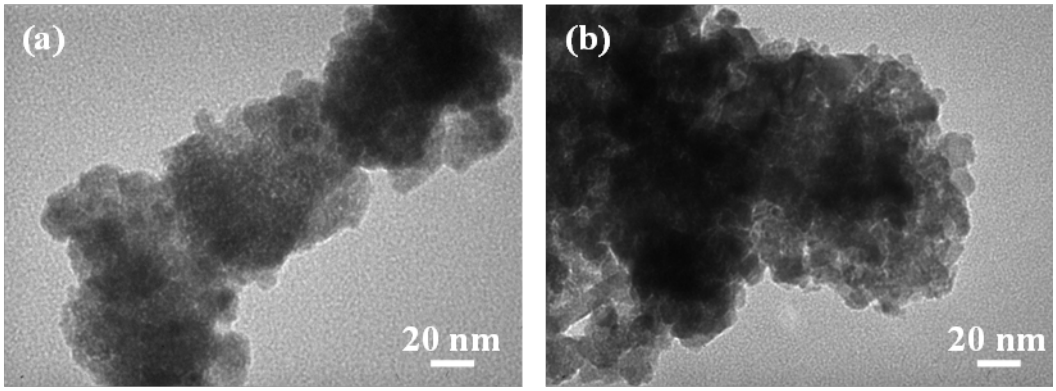

Figure 3. TEM images of the synthesized TiO_2 catalysts with (a) TiO_2_1_2, (b) TiO_2_$TiCl_4$.

Furthermore, the TiO_2_1_4 sample displayed similar physical properties to the TiO_2_$TiCl_4$ sample in terms of pore volume, pore size, and crystalline diameter, as observed in Fig. 1, Fig. 2, and Table 1. Notably, the TiO_2_1_5 sample possessed the highest specific surface area (192 m^2/g) and the smallest crystalline diameter (5.1 nm). Therefore, the facile sol-gel method employing titanium metal and oxalic acid as the chelating agent proved to be effective in producing excellent TiO_2 nanomaterials.

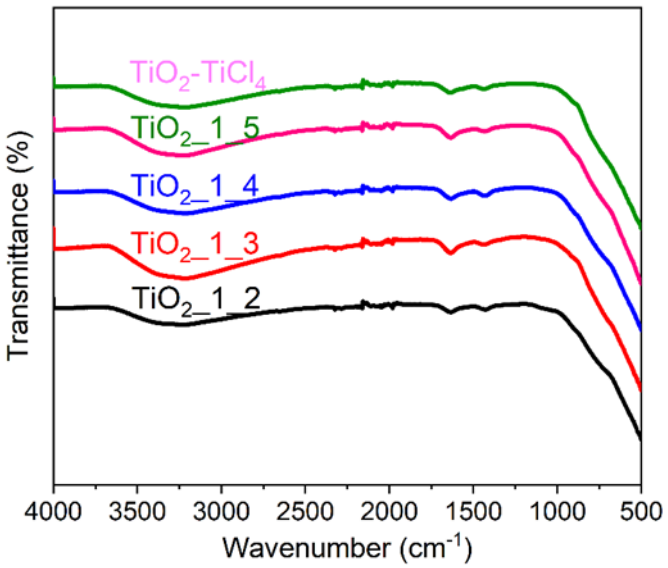

Figure 4. Infrared spectra of the synthesized TiO_2 catalysts: TiO_2_1_2; TiO_2_1_3; TiO_2_1_4; TiO_2_1_5; TiO_2_$TiCl_4$.

3.1.2. FTIR Analysis

A sequence of FTIR spectra for TiO_2_1_2, TiO_2_1_3, TiO_2_1_4, TiO_2_1_5, and TiO_2_$TiCl_4$ is presented in Figure 4. The FTIR spectra of all TiO_2 catalysts exhibit three distinct bands. The first band, observed at 3265 cm^{-1}, is the broadest and corresponds to the stretching vibration of the hydroxyl group O-H in the TiO_2 nanoparticles. The second band appears around 1635 cm^{-1} and corresponds to the bending modes of water Ti-OH. Lastly, a prominent peak at 1430 cm^{-1} is observed, which is associated with Ti-O modes occurring after the TiO_2 comes into contact with water [15].

3.1.3. UV–Visible diffuse reflectance spectra

To under

samples, the

(UV–Vis DRS) were conducted (Figure 5). The band-gap energy (E_g) of the fabricated samples could be calculated from UV-vis spectroscopy by using the Equation (2):

$$E_g = 1240/\lambda, \quad (2)$$

where λ is the wavelength (nm). It was found that Degussa P25 TiO_2, and TiO_2_$TiCl_4$ exhibited a sharp absorbance edge at about 387 nm (3.20 eV), and 391 nm (3.17 eV) and with absorbance in the UV region. Nevertheless, the absorbance edge of all as-prepared TiO_2 samples from titanium metal with different oxalic acid molar ratios (TiO_2_1_2, TiO_2_1_3, TiO_2_1_4, TiO_2_1_5) shifted toward the visible region. Moreover, the shift of the absorbance edge to the visible-light region increased gradually with the increase in oxalic acid molar ratio of 2-4 and induction of oxygen vacancies. The band gap energies of TiO_2_1_2, TiO_2_1_3, TiO_2_1_4, and

r absorbance

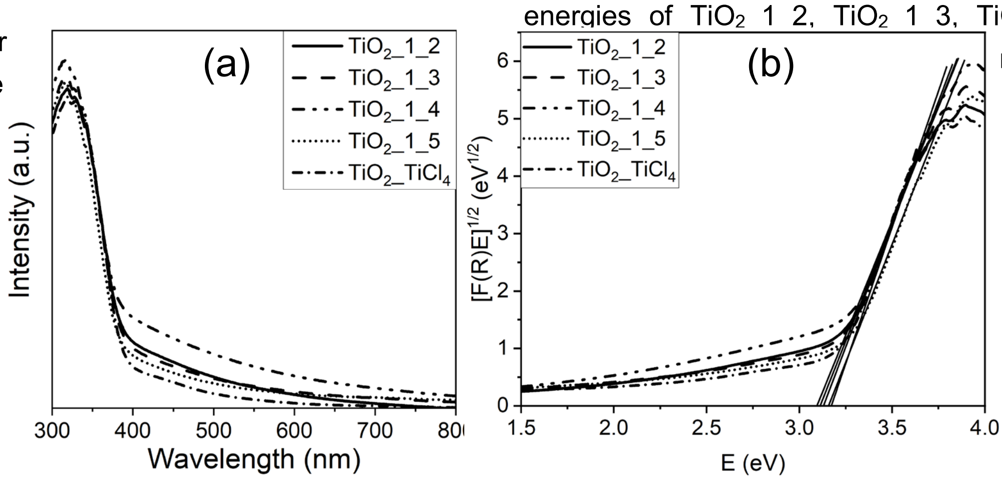

Figure 5. (a) UV–vis diffuse reflectance spectra of the synthesized TiO_2 catalysts with TiO_2_1_2; TiO_2_1_3; TiO_2_1_4; TiO_2_1_5; TiO_2_$TiCl_4$, (b) Plot of the Kubelka–Munk function plotted against the energy of absorbed light.

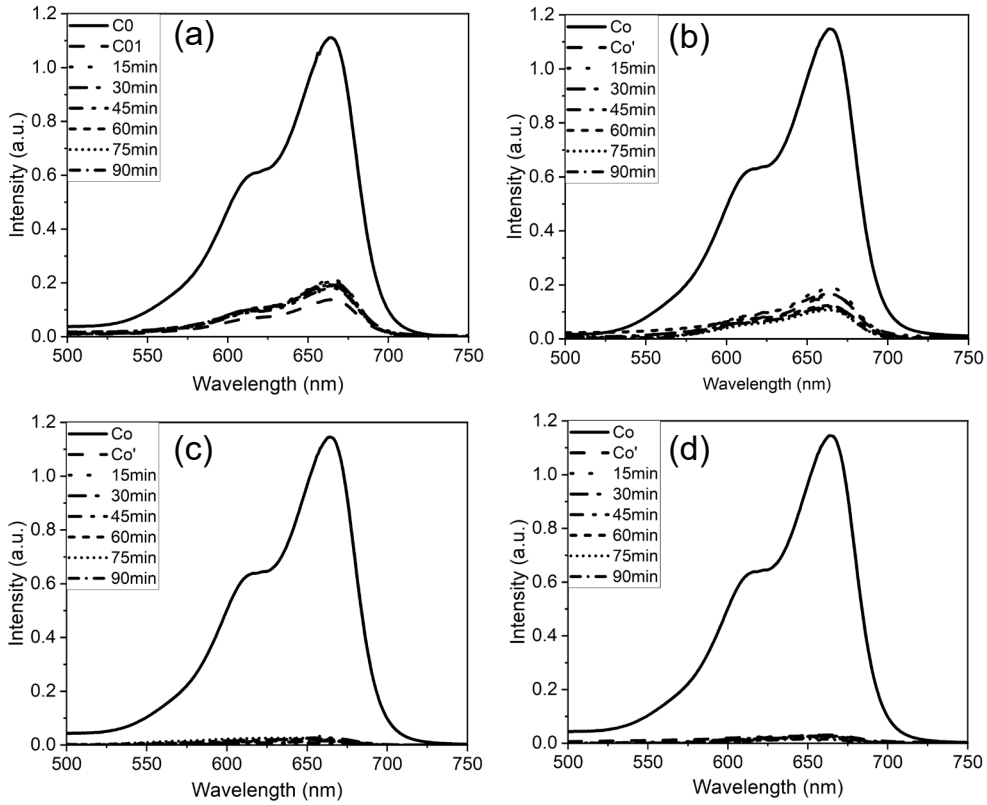

Figure 6. Absorption spectra of metylene blue dye degraded by (a) TiO_2_P25, (b) TiO_2_$TiCl_4$, (c) TiO_2_1_2 and (d) TiO_2_1_4.

Table 1. Textural properties of TiO_2-based catalysts measured by N_2 adsorption-desorption/XRD.

Catalyst	Specific Surface Area (m^2 g^{-1})	Pore Volume (cm^3 g^{-1})	Pore Size (nm)	Average Crystallite Size [a] (nm)
TiO_2_$TiCl_4$	161	0.36	7-8	10.2
TiO_2_1_5	192	0.27	6-7	5.1
TiO_2_1_4	109	0.36	10-12	10.9
TiO_2_1_3	115	0.25	7-9	13.1
TiO_2_1_2	83	0.07	4-5	14.3
TiO_2_P25	54	0.13	3.89	-

[a] Calculated by Scherrer's equation with (101) reflection of TiO_2.

edges were 3.11 eV (399 nm), 3.13 eV (396 nm), 3.09 eV (402 nm) and 3.15 eV (394 nm), respectively. The extended absorption into the visible range was likely due to the reduction of the band gap resulting from the increased charge transfer owing to the defect levels that formed in the TiO_2 band structure by oxalic acid reagent [16,17]. From these results, it was inferred that the as-prepared TiO_2 photocatalyst via a facile sol-gel method using titanium metal and oxalic acid as the chelating agent could be activated effectively under daylight irradiation.

3.2. Photocatalytic Performace

The synthesized photocatalysts were examined for their photocatalytic activities by measuring the decomposition efficiencies of metylene blue under irradiation from a 200 W tungsten lamp. Within 3 minutes of introducing the dye solution, the catalysts

successfully adsorbed the target metylene blue pollutants. Photodegradation efficiencies for metylene blue were evaluated over a 90-minute photocatalytic reaction using TiO_2_P25, TiO_2_$TiCl_4$, TiO_2_1_2, and TiO_2_1_4, as depicted in Figure 6. Remarkably, the photocatalytic degradation of the target compounds was nearly completed within the initial 15 minutes of the reaction. The degradation efficiencies achieved by TiO_2_1_2 and TiO_2_1_4 were superior to those of TiO_2_P25 and TiO_2_$TiCl_4$ in terms of adsorption capacity and photocatalytic performance under visible light. TiO_2_P25 and TiO_2_$TiCl_4$ exhibited negligible activity under visible light irradiation. Notably, both TiO_2_1_2 and TiO_2_1_4 samples demonstrated almost 100 % degradation efficiency within 15 minutes. The photocatalytic degradation efficiencies of the target compounds followed the order: TiO_2_1_4 > TiO_2_1_2 > TiO_2_$TiCl_4$ > TiO_2_P25, which correlated with the surface area, particle size, and crystallite size of the anatase phase of the synthesized TiO_2 photocatalysts, as shown in Table 1. These results indicate that the surface area and vacancies play a significant role in enhancing the photocatalytic activity of the catalysts [11,17].

4. CONCLUSION

By employing a green sol-gel method utilizing a novel titanium oxalate complex, anatase TiO_2 NPs were successfully synthesized, offering precise control over their crystalline structure and morphology. These synthesized TiO_2 NPs exhibited exceptional light absorption in the visible spectrum and demonstrated remarkable photocatalytic performance when exposed to visible light, particularly in the degradation of methylene blue. Among the various TiO_2 photocatalysts prepared, the TiO_2_1_4 sample showcased the most superior photocatalytic activity under visible light irradiation, the opposite is true of TiO_2_P25 and TiO_2_$TiCl_4$. This heightened photocatalytic activity can be attributed to the contribution of the large surface area and the oxygen vacancies within the synthesized TiO_2 catalyst.

ACKNOWLEDGEMENT

This work was supported by a research grant funded by Vietnam Ministry of Education and Training (Grant No. B2021-BKA-19).

REFERENCES

1. N. Genç, E. C. Dogan; *Adsorption kinetics of the antibiotic ciprofloxacin on bentonite, activated carbon, zeolite, and pumice,* Desalination Water Treat., 53, 2015, 785-793.
2. M. B. Ahmed, J. L. Zhou, H. H. Ngo, W. Guo; *Adsorptive removal of antibiotics from water and wastewater: Progress and challenges*, Sci. Total Environ., 532, 2015, 112-126.
3. P. Liu, H. Zhang, Y. Feng, C. Shen, F. Yang; *Integrating electrochemical oxidation into forward osmosis process for removal of trace antibiotics in wastewater*, J. Hazard. Mater., 296, 2015, 248-255.
4. L. F. Greenlee, D. F. Lawler, B. D. Freeman, B. Marrot, P. Moulin; *Reverse osmosis desalination: Water sources, technology, and today's challenges*, Water res., 43, 2009, 2317-2348.
5. B. Li, T. Zhang; *Biodegradation and Adsorption of Antibiotics in the Activated Sludge Process*, Environ. Sci. Technol., 44, 2010, 3468-3473.
6. K. E. O'Shea, D. D. Dionysiou; *Advanced Oxidation Processes for Water Treatment*, J. Phys. Chem. Lett., 3(15), 2012, 2112–2113.
7. A. Fujishima, K. Honda; *Electrochemical Photolysis of Water at a Semiconductor Electrode*, Nature, 238, 1972, 37–38.

8. A. Kudo, Y. Miseki; *Heterogeneous photocatalyst materials for water splitting*, Chem. Soc. Rev., 38, 2009, 253–278.

9. J. Schneider, M. Matsuoka, M. Takeuchi, J. Zhang, Y. Horiuchi, M. Anpo, D. W. Bahnemann; *Understanding TiO_2 Photocatalysis: Mechanisms and Materials*, Chem. Rev., 114(19), 2014, 9919–9986.

10. M. Kobayashi, V. V. Petrykin, M. Kakihana; *One-Step Synthesis of TiO_2(B) Nanoparticles from a Water-Soluble Titanium Complex*, Chem. Mater., 19, 2007, 5373-5376.

11. Q. D. Truong, L. X. Dien, D.-V. N. Vo, T. S. Le; *Controlled synthesis of titania using water-soluble titanium complexes: A review*, J. Solid State Chem., 251, 2017, 143–163.

12. G. M. H. Van De Velde, S. Harkema, P. J. Gellings; *The Crystal and Molecular Structure of Ammonium Titanyl Oxalate*, Inorganica Chim. Acta., 11, 1974, 243–252.

13. Y. F. You, C. H. Xu, S. S. Xu, S. Cao, J. P. Wang, Y. B. Huang, S. Q. Shi; *Structural characterization and optical property of TiO_2 powders prepared by the sol–gel method*, Ceram. Int., 40(6), 2014, 8659-8666.

14. C. Ai, X. Wu, Y. Ke, Y. Lei, X. Shao; *Synthesis and Photocatalytic Sterilization Performance of SA/TiO_2*, J. Inorg. Organomet. Polym. Mater., 30, 2020, 3378–3387.

15. H. Park, T. Goto, S. Cho, S. W. Lee, M. Kakihana, T. Sekino; *Effects of Annealing Temperature on the Crystal Structure, Morphology, and Optical Properties of Peroxo-Titanate Nanotubes Prepared by Peroxo-Titanium Complex Ion*, Nanomater., 10, 2020, 1331.

16. K. Katsumata, Y. Ohno, K. Tomita, M. Sakai, A. Nakajima, M. Kakihana, A. Fujishima, N. Matsushita, K. Okada; *Preparation of TiO_2 Thin Films Using Water-soluble Titanium Complexes and Their Photoinduced Properties*, Photochem. Photobiol., 87, 2011, 988–994.

17. L. Li, X. Chen, L. Wang, C. Tao, X. Wu, J. Du, Z. Liu; *Synthesis of Ti^{3+} self-doped mesoporous TiO_2 cube with enhanced visible-light photoactivity by a simple reduction method*, J. Alloys Compd., 845, 2020, 156138.